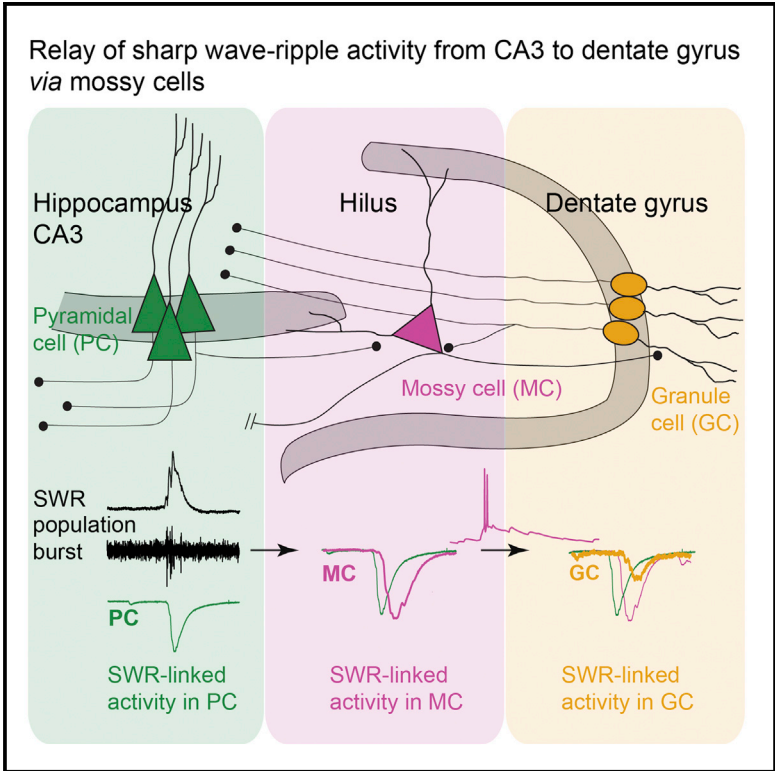


Cell Reports

Involvement of Mossy Cells in Sharp Wave-Ripple Activity *In Vitro*

Graphical Abstract



Authors

Aarti Swaminathan, Ines Wichert, Dietmar Schmitz, Nikolaus Maier

Correspondence

nikolaus.maier@charite.de

In Brief

The functional implication of hippocampal mossy cells (MCs) is thus far poorly understood. Swaminathan et al. demonstrate sub-threshold activity and recruitment of MCs during ripples that are fast neuronal oscillations involved in memory consolidation. These results suggest a pivotal role for MCs in computations occurring during ripple-related brain states.

Highlights

- Mossy cells (MCs) receive ripple-related excitatory and inhibitory synaptic inputs
- These inputs occur at high fidelity and are phase coherent with ripples
- Ripple-related synaptic activity can recruit MCs into the active network
- MC spiking can give rise to ripple-associated synaptic inputs in granule cells



Involvement of Mossy Cells in Sharp Wave-Ripple Activity *In Vitro*

Aarti Swaminathan,^{1,4} Ines Wichert,² Dietmar Schmitz,^{1,2,3,4,5,6,7} and Nikolaus Maier^{1,7,8,*}¹Charité-Universitätsmedizin Berlin, corporate member of Freie Universität Berlin, Humboldt-Universität zu Berlin, and Berlin Institute of Health, Neuroscience Research Center, 10117 Berlin, Germany²Bernstein Center for Computational Neuroscience Berlin, 10115 Berlin, Germany³Berlin Institute of Health, 10178 Berlin, Germany⁴Cluster of Excellence NeuroCure, 10117 Berlin, Germany⁵German Center for Neurodegenerative Diseases (DZNE) Berlin, 10117 Berlin, Germany⁶Einstein Center for Neurosciences Berlin, 10117 Berlin, Germany⁷Senior author⁸Lead Contact*Correspondence: nikolaus.maier@charite.de<https://doi.org/10.1016/j.celrep.2018.04.095>

SUMMARY

The role of mossy cells (MCs) of the hippocampal dentate area has long remained mysterious. Recent research has begun to unveil their significance in spatial computation of the hippocampus. Here, we used an *in vitro* model of sharp wave-ripple complexes (SWRs), which contribute to hippocampal memory formation, to investigate MC involvement in this fundamental population activity. We find that a significant fraction of MCs (~47%) is recruited into the active neuronal network during SWRs in the CA3 area. Moreover, MCs receive pronounced, ripple-coherent, excitatory and inhibitory synaptic input. Finally, we find evidence for SWR-related synaptic activity in granule cells that is mediated by MCs. Given the widespread connectivity of MCs within and between hippocampi, our data suggest a role for MCs as a hub functionally coupling the CA3 and the DG during ripple-associated computations.

INTRODUCTION

The hippocampal dentate gyrus (DG) is considered the input structure where information from the entorhinal cortex is processed. The most abundant excitatory neurons in the DG, the granule cells (GCs), forward this input to the CA3 region via mossy fibers (Lorente de Nó, 1934; Henze et al., 2000). On their way to the CA3 area, mossy fibers contact the second population of glutamatergic cells in the DG, mossy cells (MCs), whose somata reside in the hilus (Amaral, 1978; Berger et al., 1981; Scharfman et al., 1990; Soriano and Frotscher, 1994). In addition to excitatory inputs from GCs, MCs receive inhibitory inputs from local interneurons and excitatory “back” projections from CA3 pyramidal cells (PCs) (Scharfman, 1994c; Acsády et al., 2000; Larimer and Strowbridge, 2008). The dendrites of MCs are

confined mostly to the hilus, but some extend to the molecular layer of the DG (Frotscher et al., 1991). MC axons ramify within the hilus and project to the inner molecular layers of both the ipsi- and the contralateral DG (Berger et al., 1981; Ribak et al., 1985; Buckmaster et al., 1996; Hsu et al., 2016). Taken together, these anatomical features suggest a strategic role for MCs in relaying information in the CA3-DG network, within and between hemispheres.

Recent studies have started to elucidate the activity of MCs across different behaviors (Neunuebel and Knierim, 2012; Danielson et al., 2017; GoodSmith et al., 2017). Specifically, MCs were shown to display higher firing rates during slow-wave sleep (SWS) compared with rapid eye movement (REM) sleep and alert behaviors (Senzai and Buzsáki, 2017). In the hippocampal electroencephalogram (EEG), SWS and quiet wakefulness are characterized by transient field events in the CA3 to CA1 regions, termed sharp waves, that occur in association with high-frequency (~120–250 Hz) ripple oscillations (sharp wave-ripple complexes [SWRs]; Buzsáki, 1986; for review see Buzsáki, 2015). During SWRs, neuron sequences previously active during behavior are re-activated, and this “replay” of activity is thought to support memory consolidation (Lee and Wilson, 2002; Girardeau et al., 2009; Jadhav et al., 2012).

The role of MCs in the context of SWRs remains unclear. Given the technical challenges of targeting MCs *in vivo*, a slice model of SWRs provides an attractive experimental system to investigate MCs during SWRs. Acute hippocampal slices can express sharp waves and ripples autonomously, in physiological bathing solutions, without drugs that elevate the network excitability (Maier et al., 2003, 2009, 2011; Both et al., 2008; Hájos et al., 2009, 2013; Papatheodoropoulos and Kostopoulos, 2002; Kubota et al., 2003; for review, see Maier and Kempter, 2017).

Here, we used this *in vitro* tool to elucidate MC activity during SWRs in acute slices of the mouse hippocampus. We identified SWR-associated synaptic currents in MCs and the recruitment of MCs into the active network. Taken together, our results suggest that SWR-associated information is relayed by MCs from CA3 “backward” into the network of the DG.



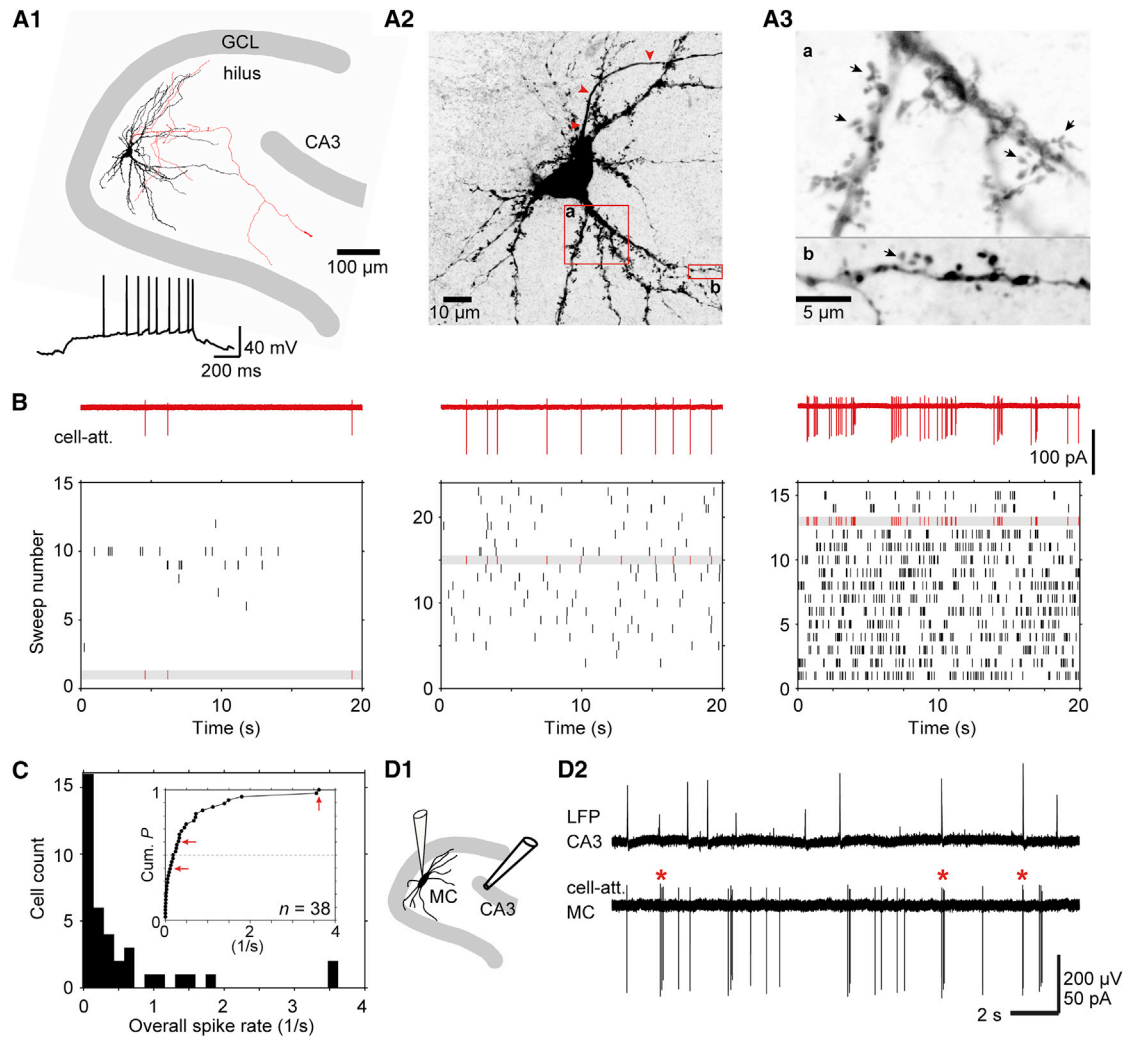


Figure 1. Spontaneous MC Activity in Mouse Hippocampal Slices

(A1) Reconstruction of a biocytin-filled MC. Dendrites in black, the axon in red. Below: the firing pattern during a 40 pA (1 s) current injection. (A2) Confocal image showing complex spines on the proximal dendrites. Arrowheads mark the axon. (A3) Magnification of the boxed areas in (A2) to visualize spines at higher resolution (arrows). (B) Example recordings (top) and raster plots of successive sweeps show varied discharge behaviors in MCs. (C) Histogram of overall spike rates. Inset: cumulative distribution of firing rates; red arrows indicate the cells shown in (B). (D1) Sketch to illustrate parallel LFP-MC recordings. (D2) Example showing the CA3 LFP and MC spiking. Asterisks indicate MC discharge concurrent with SWRs.

RESULTS

Properties of MCs

Across species and behavioral conditions, MCs have been shown to be a highly active class of hippocampal excitatory neurons (Henze and Buzsáki, 2007; GoodSmith et al., 2017; Senzai and Buzsáki, 2017). We used acute brain slices to study neuronal network mechanisms underlying MC activity. With differential interference contrast microscopy, we identified putative MCs as multipolar cells located in the hilus and outside the CA3c PC layer (Buckmaster et al., 1993; Figure 1A1). To identify MCs, all cells were biocytin labeled during recording and confirmed post hoc on the basis of morphological features. In

particular, MCs exhibit a high density of large, complex spines (“thorny excrescences”) on their proximal dendrites and soma (Figures 1A2 and 1A3; Amaral, 1978; Ribak et al., 1985). We used this property as a defining criterion, and consequently, only cells expressing thorny excrescences were included in our analysis. In addition, none of the included cells expressed the GABAergic marker GAD67 (Figure S1A). Stained axon collaterals of MCs were found in the hilus and the inner molecular layer, and often, cells displayed a major axon collateral extending toward the stratum oriens of CA3 (Figure 1A1; Amaral, 1978; Buckmaster et al., 1996). Electrophysiological properties of MCs are summarized in Figure S1B and were comparable with those of murine MCs reported by others (Kowalski et al., 2010).

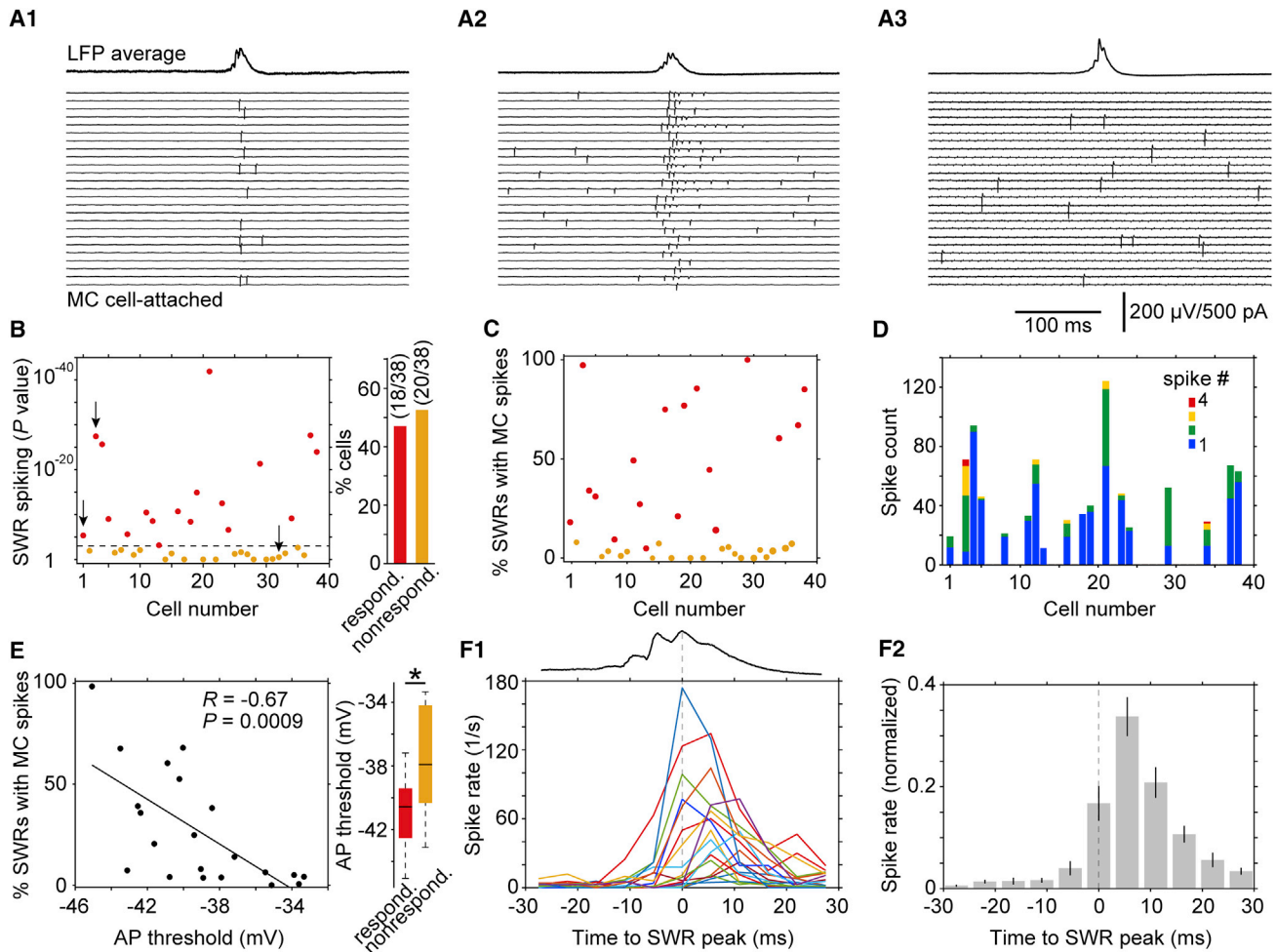


Figure 2. Analysis of MC Activity during CA3 SWRs

(A1–A3) Discharge patterns of three MCs during CA3 SWRs. Successive sweeps (25 and 400 ms) centered to the SWR peak (average top).
 (B) Spiking of MCs within and outside SWR epochs was compared (Mann-Whitney U test). Left: display of p values (x axis, order of experiments). Red and orange dots indicate a significant increase (responding) or no significant increase (nonresponding) in spike rate during SWRs; dotted line, $\alpha = 0.001$; arrows, cells shown in (A1–A3). Right: distribution of responding and nonresponding MCs.
 (C) Numbers of SWR epochs with MC spiking divided by total number of SWR epochs per experiment shown as percentages (x axis and color as in B).
 (D) Distribution of mean spike counts per SWR for responding cells (order as in B and C).
 (E) Left: correlation analysis of MC spiking and AP threshold ($n = 21$). Right: lower AP threshold in responding cells; error bars represent 10th and 90th percentiles.
 (F1) PETHs of responding MCs, 5 ms bin size. Top: grand average SWR.
 (F2) Average PETH after normalization (peak at 6.4 ms). Error bars represent SEM.

Non-invasive recordings from MCs (depth 32–80 μm ; Figures S1C–S1D) revealed spontaneous and heterogeneous action potential (AP) firing as illustrated in raster plots of three cells (Figure 1B). The distribution of the overall spike rates is given in Figure 1C (mean $0.5 \pm 0.1/\text{s}$, median 0.2/s, range 0–3.6/s; $n = 38$ cells).

MCs are known to receive excitatory synaptic input at high rates, mostly from GC axons (Scharfman et al., 1990; Strowbridge et al., 1992) but potentially also from “feedback” projections originating from CA3 pyramidal neurons (Scharfman, 1994c). We asked whether the observed MC spiking could potentially reflect SWR-associated activity arising from CA3.

MC Activation during SWRs

We recorded the local field potential (LFP) in the PC layer of area CA3c (Lorente de Nó, 1934) together with activity from MCs, and we indeed observed spikes coinciding with SWRs in a substantial fraction of MCs (Figure 1D), suggesting recruitment of these neurons by population activity in the adjacent CA3.

Patterns of MC spiking observed in peri-SWR epochs are shown in Figure 2A. To statistically evaluate a causal relation between MC spiking and SWRs in CA3, we compared the spiking during SWRs with spiking during randomly sampled periods (Mann-Whitney U test; Figure 2B). Of 38 MCs, the spiking in 18 cells (47%) was significantly coupled with SWRs (“responding”),

while for the remaining cells (53%), no coupling could be found, or they were mostly silent (“nonresponding”; Figures S2A–S2E). In the responding MCs, SWR-linked spiking for individual cells varied between ~5% and 100% (Figure 2C), independent of the recording depth from the slice surface (Figure S2F). In addition, the number of spikes per SWR ranged from one to four (mean 1.4 ± 0.02 ; Figure 2D). We tested several intrinsic and network parameters that might account for differences in responding and nonresponding MCs. None of these measures were different (Figures S2G and S2H) with the exception of AP threshold, which was negatively correlated with SWR-related spiking (Figure 2E, left). Specifically, the AP threshold was more negative in responding MCs, implying that synaptic activity would evoke spikes at a higher probability (Figure 2E, right; $p = 0.017$, two-tailed unpaired t test).

We analyzed the distribution of spike times with respect to the SWR peak time as a common temporal reference across cells. Figure 2F displays the SWR-locked peri-event time histograms (PETHs), individually for all responding cells (trial-averaged spike rates; Figure 2F1) and the average after normalization (Figure 2F2). Across cells, the peak firing of MCs was delayed with respect to the SWR peak (6.4 ms; Figure 2F2), demonstrating a delayed recruitment of MCs into the active neuronal network during SWRs in the adjacent CA3 area.

SWR-Related Synaptic Inputs in MCs Are Reliable and Phase Locked

Given the substantial fraction of active MCs, we were interested in exploring the underlying synaptic activity. We sequentially recorded, from the same cells, compound excitatory postsynaptic currents (cEPSCs) and compound inhibitory postsynaptic currents (cIPSCs) (cEPSCs at -60 mV, cIPSCs at $+6$ mV) concurrently with CA3 SWRs. Figure 3 illustrates features of these currents: excitatory and inhibitory compound postsynaptic current (cPSC) amplitudes were in the range of several hundreds of picoamperes (cEPSCs: mean 644 ± 70 pA, median 679 pA; cIPSCs: mean 509 ± 50 pA, median 520 pA; $n = 25$ cells; see also Figure S3A). In addition, SWR-related cPSCs in MCs were highly reliable, with success rates of 100% and 97% for cEPSCs and cIPSCs (Figure S3A). Spectral analysis of both components revealed frequencies consistent with the ripple frequency (cEPSCs versus cIPSCs: mean 144 ± 1 Hz versus 144 ± 2 Hz, median 143 Hz versus 142 Hz, $p = 0.9$, Mann-Whitney U test; Figure 3B), supported by amplitude-time histograms of cPSCs indicating ~5 ms rhythmicity (Figure S3B).

We have previously shown the coherence of synaptic inputs in CA1 PCs, and in oriens-lacunosum moleculare (O-LM) interneurons with ripples *in vitro* (Maier et al., 2011; Pangalos et al., 2013; see Hájos et al., 2013, for similar results in CA3). We wondered whether such coupling was also present between CA3 ripples and related synaptic input in MCs (Figure 3C). In data obtained from 25 MCs, we found significant phase locking with the CA3 ripple for both cEPSCs and cIPSCs ($p < 1 \times 10^{-8}$ and $p < 9 \times 10^{-7}$, Rayleigh test; Figure 3D). Comparison of the average phases revealed a lead of excitatory over inhibitory synaptic inputs (cEPSC- and cIPSC-to-ripple phase: $14.3 \pm 8.2^\circ$ [vector strength 0.29] versus $39.2 \pm 9.9^\circ$ [vector strength 0.26]; see also Figure S3C).

Scharfman (1994c) showed unitary synaptic connections from CA3 PCs onto MCs with time-to-peak latencies in the range of

3.5–8.5 ms. To quantify the propagation time of SWR-related synaptic activity to MCs, we performed cross-correlation analyses of cPSCs with CA3 SWRs. Consistent with the previously reported monosynaptic delays, we found time lags of ~5 ms for cEPSCs (mean 4.8 ± 0.3 ms, median 4.9 ms; 1,214 events; Figure 3E1), while time lags for cIPSCs were prolonged (mean 5.9 ± 0.4 ms, median 5.7 ms, 1,187 events; $p = 0.0005$, paired two-tailed t test; $n = 25$ cells; Figure 3E2).

To corroborate these propagation delays with an additional approach, we performed simultaneous recordings from PCs and MCs with the CA3 LFP. Figure 3F1 displays the ripple peak-triggered averages of SWRs and corresponding cEPSCs and cIPSCs in both a PC and an MC (green and orange; reconstructions; Figure 3F2). In 15 such recordings, we found consistently delayed cPSCs in MCs compared with PCs (cEPSC delays: mean 3.8 ± 0.5 ms, median 3.6 ms, 1,224 events; cIPSC delays: mean 5.9 ± 0.7 ms, median 5.7 ms, 1,598 events; Figure 3F3). Moreover, inhibitory latencies were prolonged compared with excitatory latencies ($p = 0.006$, paired two-tailed t test; Figure 3F3, bottom).

Together, these findings confirm the precise signaling and delayed propagation of ripple-related synaptic activity from the CA3 network to MCs.

SWR-Linked Excitatory Synaptic Activity Is Routed to GCs via MCs

Within the local network, MC spiking has been shown to evoke excitatory postsynaptic responses in DG GCs and in hilar interneurons (Scharfman, 1995; Larimer and Stowbridge, 2008). We were thus interested in testing whether SWR-related activity in CA3 is relayed on to GCs, potentially via active MCs. Indeed, we observed significant SWR-associated excitatory and inhibitory synaptic inputs in GCs (cEPSCs and cIPSCs: 19 of 29 [66%] and 13 of 22 [60%] GCs; Figure S4A). To investigate the timing of SWR-related synaptic activity in MCs and in GCs, we simultaneously recorded from cells of both groups, together with the CA3c LFP (Figure 4A). We found that SWR-associated cEPSCs in GCs consistently lagged behind those detected in MCs (Figures 4A2 and 4A3), with an average delay of 4.2 ± 0.6 ms (median 4.1 ms; 1,266 events in 16 simultaneous recordings; Figure 4B). This delay is consistent with prolonged cross-correlation derived LFP-cEPSC time lags determined in GCs compared with MCs (Figures S4B and S4C). It supports the idea of backpropagation of SWR-linked excitatory activity from the CA3 area to the GC/dentate network via a disynaptic pathway involving MCs.

We sought to test this hypothesis using a different approach. We reasoned that the ripple-associated population activity in CA3 might be more tightly coupled with excitatory synaptic input in MCs than in GCs, given the disynaptic chain of propagation (CA3 → MC → GC) and the reported failure rates at the MC → GC synapse (22% on average; Scharfman, 1995). We used CA3 SWR amplitude as a readout parameter of the local network excitability. In 31 slices, we correlated individual SWR amplitudes with corresponding cEPSC amplitudes in PCs (see histogram of correlation coefficients in Figure 4C1). Similarly, we obtained correlation coefficients for MCs (56 slices; Figure 4C2) and GCs (38 slices; Figure 4C3). The medians of the distributions are similar for PCs and MCs (0.58 versus 0.56; red lines) but considerably lower for GCs (0.18). We obtained

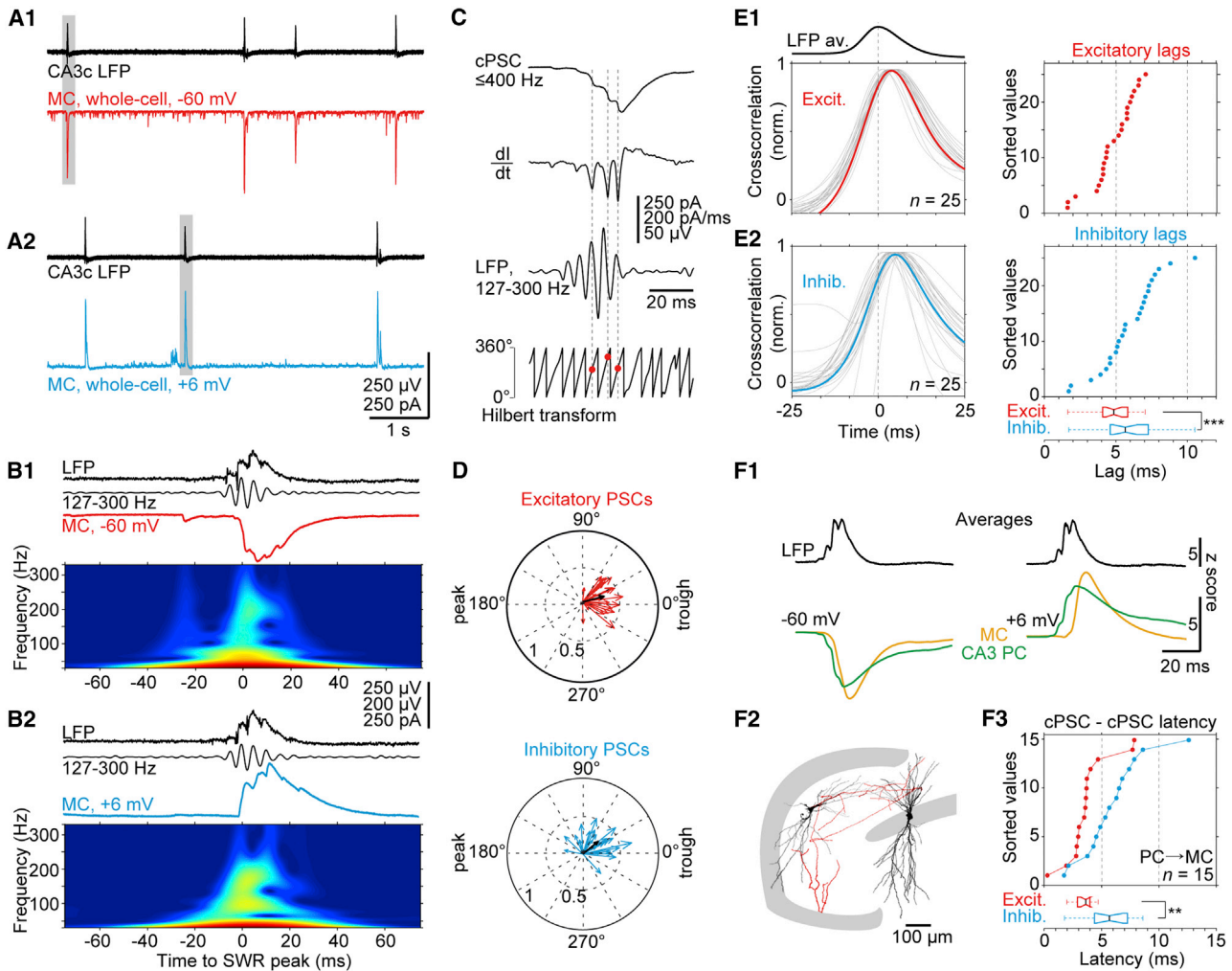


Figure 3. Timing of Ripple-Linked cPSCs in MCs

(A1 and A2) SWRs in CA3c (top) linked with cEPSCs and cIPSCs in MCs (red and blue). (B1 and B2) Events marked in (A1) and (A2) at higher resolution; top to bottom: LFP SWR, filtered version, and cEPSC (red) and cIPSC (blue). Below: wavelet spectrograms of the cEPSC and cIPSC; warmer colors represent higher power. (C) Analysis of cPSC-to-ripple phases. Top: time points of steepest rising slopes in cPSC identified by their first derivatives (middle). The phases of these time points were determined with respect to the ripple (LFP) using its Hilbert phase (red dots, bottom). In total, 2,770 excitatory and 3,012 inhibitory slopes were analyzed. (D) Polar plots of average phases of excitatory (red) and inhibitory (blue) PSCs (slopes) of each cell with respect to CA3 ripples; black arrows: resultant phase vectors. (E1 and E2) Left, cross-correlation (CC) analysis of cEPSCs (E1) and cIPSCs (E2); single (gray) and averaged (red and blue) CC functions, aligned to peak of SPW envelope (top). Right: median SPW-cPSC time lags for cEPSCs (red) and cIPSCs (blue). Bottom: cIPSCs are delayed compared with cEPSCs. (F1-F3) Simultaneous PC-MC recordings during CA3c SWRs. (F1) Ripple peak-triggered averages of 100 SWRs (top) and their excitatory (left) and inhibitory (right) cPSCs (PC, green; MC, orange; reconstruction; F2). (F3) Median latencies for cEPSCs (red) and cIPSCs (blue). Inhibitory compared with excitatory latencies are consistently delayed in simultaneously recorded PCs and MCs (bottom). (E2) (bottom right) and (F3) (bottom): error bars represent 10th and 90th percentiles.

transformed Fisher's Z values to statistically compare these data and found no difference for Z values representing LFP-PC and LFP-MC correlations ($p = 0.94$, Tukey's multiple-comparisons test), while Z values representing LFP-GC correlations were significantly smaller ($p < 0.0001$ for both comparisons, Tukey's multiple-comparisons test; Figure 4D).

Together, these results demonstrate that during SWRs, network activity is equally linked with excitatory signaling in PCs and MCs but not in GCs. This rejects a strong role for direct

functional coupling of CA3 PCs and GCs (Li et al., 1994) during ripples but supports an indirect propagation of SWR-related excitatory activity onto GCs via MCs.

DISCUSSION

Despite recent progress in elucidating their behavioral relevance (Jinde et al., 2012; Danielson et al., 2017; GoodSmith et al., 2017; Senzai and Buzsáki, 2017), MCs remain a comparatively

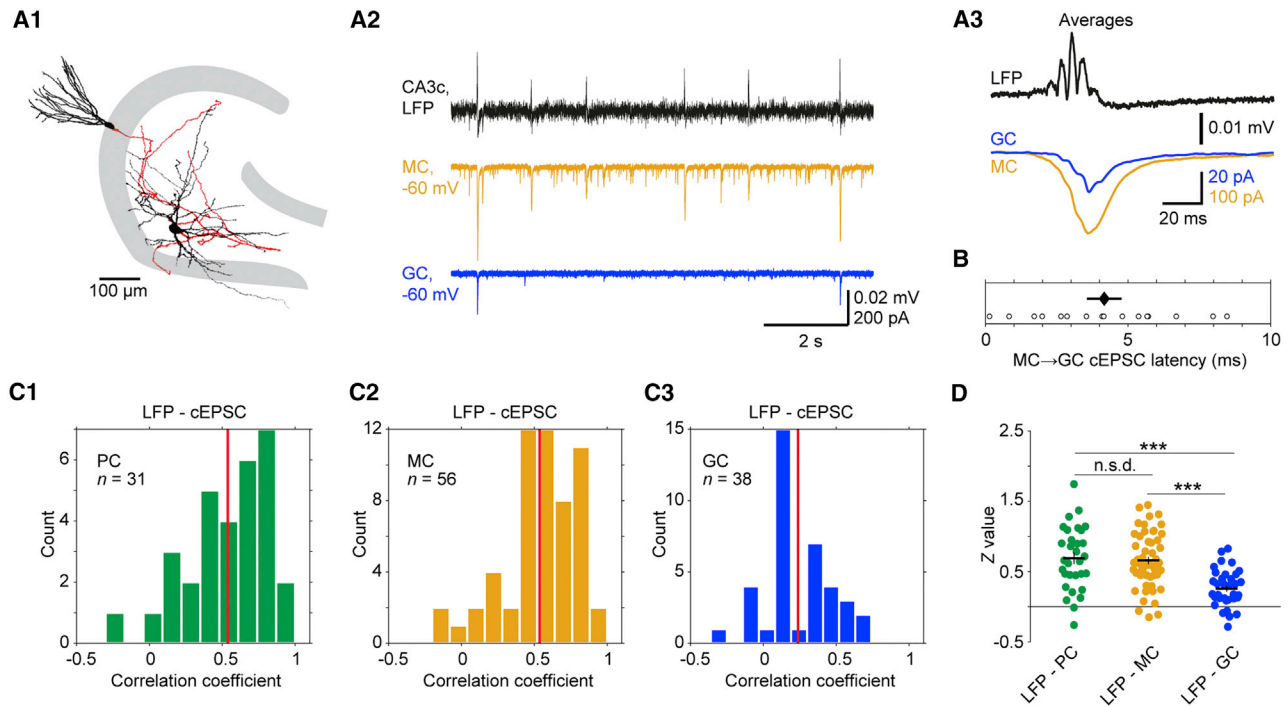


Figure 4. Ripple-Associated Functional Coupling of CA3 and GCs via MCs

(A1) Reconstruction of simultaneously recorded MC and GC.

(A2) Example sweeps, same experiment as (A1). Top: CA3c SWR and corresponding cEPSCs in MC (orange) and GC (blue).

(A3) Ripple peak-triggered average of 100 SWRs (top) and corresponding cEPSCs (as A1 and A2).

(B) Median latencies (16 MC-GC recordings; diamond, average). The error bar represents SEM.

(C1–C3) Correlation of CA3c SWR and cEPSC amplitudes in PCs (C1), MCs (C2), and GCs (C3). Histograms of Pearson correlation coefficients for amplitudes of SWRs and cEPSCs in CA3 PCs (31 slices, 2,231 SWRs; C1), MCs (56 slices, 3,695 SWRs; C2), and GCs (38 slices, 2,326 SWRs; C3). Red lines, population medians.

(D) Comparison of Fisher's Z values. Dots, Z-transformed correlation coefficients from the histograms in (C1)–(C3). Error bars represent SEM.

unexplored neuron population, especially regarding their differential role in various brain states. This is due mainly to their relatively low density deep in the hilus (1–5 MCs per 100 GCs, i.e., ~10,000 MCs in the rat; Henze and Buzsáki, 2007; Myers and Scharfman, 2009) and their particular vulnerability, which impedes *in vivo* recording and post hoc anatomical identification (Scharfman and Myers, 2013; GoodSmith et al., 2017). Here, we took advantage of an *in vitro* approach whereby SWRs can be studied in isolation and at the single-cell level to investigate MCs in a targeted way. *In vitro* SWRs share multiple properties with their *in vivo* counterparts, including their spatial and spectral profiles, pharmacology, and activation patterns of participating neurons (Maier et al., 2009; Koniaris et al., 2011; Hájos et al., 2013; Pangalos et al., 2013; for review, see Maier and Kempter, 2017).

We identified prominent excitatory postsynaptic currents in MCs that consistently followed SWRs in CA3c. This finding implies a transient functional coupling of MCs with the CA3 area during SWRs. As an anatomical substrate underlying this coupling, a monosynaptic excitatory “back-projection” from CA3 pyramidal neurons onto MCs has been demonstrated with paired intracellular recordings (Scharfman, 1994c). In these unitary connections, the time of spike to excitatory postsynaptic potential (EPSP) was comparable with the time lags we observed for CA3 LFP and cEPSCs in MCs, which we further substantiated

by simultaneous cEPSC recordings in PCs and MCs. Together, these results suggest that ensembles of rhythmically active CA3 pyramidal neurons directly provide input to MCs during SWRs.

Beside phase-locked excitatory cPSCs, we observed pronounced, phase-locked inhibitory cPSCs in MCs. Their time lags with respect to the LFP were prolonged compared with those of excitatory cPSCs. The inhibitory delays were confirmed by latencies determined in simultaneous cIPSC recordings from PCs and MCs.

Several possible explanations are conceivable for the origin of ripple-locked inhibition in MCs. (1) Recently, a novel class of GABAergic interneurons was shown to send axons from CA1/CA3 to the DG and to increase spiking during SWRs (Szabo et al., 2017). (2) In addition to these “boundary-crossing” projections, it is feasible that MCs are targeted by CA3 interneurons that are known to discharge during ripples, namely, basket, bistratified, and O-LM cells (Lasztóczy et al., 2011; Hájos et al., 2013; Tukker et al., 2013). (3) The recruitment of local hilar interneurons (Sík et al., 1997; Hosp et al., 2014) by axon collaterals of CA3 PCs constitutes another possibility. In this framework, spiking CA3 PCs activate hilar interneurons that in turn provide inhibition in MCs, as the output of a disynaptic pathway (PC → interneuron → MC). However, given the large amplitudes and

the ripple phase coupling of cIPSCs in MCs, (1) and (2) seem to be the more likely explanations.

Synaptic inputs in MCs evoked by population activity generated in CA3 have been studied *in vitro* before, but in the context of experimentally enhanced cellular excitability or epileptiform activity (Scharfman, 1994a, 1994b; Hedrick et al., 2017). Epileptiform discharges, compared with SWR activity, exhibit considerably enhanced amplitude, duration, multi-unit activity, and oscillation frequency (Karlócai et al., 2014; Aivar et al., 2014). Thus, profound differences exist between the network mechanisms that govern pathological network discharges as opposed to physiological SWRs.

We found significant activation in 47% of probed MCs, which is in contrast to the previously reported low activation of CA3 PCs during SWRs (Hájos et al., 2013). What could explain the discrepancy in the activation of these two neighboring principal neuron populations during SWRs? A characteristic feature of MCs is an ongoing “bombardment” with excitatory synaptic activity, at rates considerably higher than in CA3 PCs (Scharfman and Schwartzkroin, 1988; Strowbridge et al., 1992). This background activity might serve as an excitatory “blanket,” raising the likelihood of spiking during SWRs. In addition, Scharfman and Schwartzkroin (1988) demonstrated higher input resistance in MCs than in CA3 PCs, which contributes to cellular excitability and hence a more likely recruitment of MCs during SWRs.

Although not addressed directly so far, recent work has provided indirect evidence for MC activation during SWRs: MCs are active during SWS (Senzai and Buzsáki, 2017), which is the sleep stage characterized by a high occurrence of SWRs in the hippocampus. Our observations *in vitro* support this finding and demonstrate that the SWR-associated increased network excitability is sufficient to drive MCs.

What could be consequences of MC spiking in the neuronal network? Previous research has shown that dentate GCs, a major neural population targeted by MCs (Scharfman, 1995, 1996), are also active during SWRs (Buzsáki, 1986; Ylinen et al., 1995) and SWS (Senzai and Buzsáki, 2017). In awake mice, Hulse and colleagues (2017) have directly shown that GCs depolarize during SWRs.

We hypothesize that the discharge of MCs relays SWR-related activity to GCs, thereby contributing to the activation of these neurons. First, this reasoning is in agreement with our observation that excitatory synaptic inputs in GCs are often coupled with SWRs. Second, it is in line with the consistent delay between ripple-related cPSCs in GCs and simultaneously recorded MCs. And third, this is supported by strong correlations between CA3 SWR amplitudes and cEPSC amplitudes in both PCs and MCs, but not in GCs, demonstrating a direct connection of the CA3 excitatory oscillation generator driving PCs and MCs, but importantly not GCs. All these findings support a disynaptic chain of activity propagation (CA3 PC → MC → GC; Scharfman, 1994b).

MCs are part of an excitatory recurrent feedback network (Lisman, 1999) and placed in a strategic position to integrate information from the connected neuronal sub-networks, DG and CA3. MCs receive converging excitatory inputs from CA3 PCs and GCs and send projections in an eminently divergent fashion: ipsilaterally, along the septotemporal axis of the hippocampus,

MC axons can span hundreds of micrometers, with a greater concentration of proximal contacts in the hilus, presumably on interneurons (Larimer and Strowbridge, 2008), as opposed to an aggregation of more distant contacts in the inner molecular layer, presumably on GCs (Buckmaster et al., 1996). As a consequence, proximal GCs might be predominantly suppressed by MC-driven disynaptic inhibition (Buzsáki and Eidelberg 1981; Buckmaster et al., 1996), in contrast to distal GCs, which may be entrained by enhanced MC activity during SWRs. SWR-linked MC spiking might represent the physiological trigger to induce long-term potentiation (LTP) at the MC → GC synapse, as shown for experimental activation of MC axons (Hashimoto et al., 2017). Contralaterally, MC axons contribute to commissural terminals linking both hippocampi (Berger et al., 1981; Ribak et al., 1985; Hsu et al., 2016). It is tempting to speculate that the active MCs support, or mediate, the SWR-related synchronization of hippocampus along the septotemporal axis (Patel et al., 2013) or across hemispheres at the timescale of several milliseconds (Buzsáki, 1986; Buzsáki et al., 2003). Given the prominent innervation of GABAergic interneurons by MCs, this synchronization could be mediated by local and/or contralateral inhibitory neurons (Scharfman, 1995; Larimer and Strowbridge, 2008; Hsu et al., 2016).

Together, these features suggest the role of MCs as a neuronal hub linking local and distal compartments of both hippocampi in a complex manner. Our findings on the “feedback” recruitment of MCs strongly argue for a central role of these cells in SWR-related hippocampal functions, which include the consolidation of spatial and emotional memories (Jinde et al., 2012; Myers and Scharfman, 2009; Scharfman, 2016).

EXPERIMENTAL PROCEDURES

Animal maintenance and experiments followed institutional guidelines, the guidelines of the Berlin state (T0100/03), and European Union (EU) Council Directive 2010/63/EU on the protection of animals used for experimental and other scientific purposes. Male C57BL/6N mice (3–5 weeks of age) were used.

Slice Preparation and Electrophysiology

Horizontal slices of ventral to mid-hippocampus were prepared as described before (Maier et al., 2009). Slices were stored in an interface chamber, and combined LFP and patch-clamp (cell-attached or whole-cell) recordings were performed at 31°C–32°C in a submerged-type recording chamber.

Data Analysis

SWR detection was performed in MATLAB (The MathWorks) as described before (Maier et al., 2009). Time windows of 300 ms (55 ms for spike analysis) aligned to the peak of identified SWRs were cut out from LFP and corresponding intracellular traces and were baseline-corrected by subtracting the respective means. Digital filtering was performed with second-order Butterworth filter at the indicated frequencies.

Spike times were detected using a threshold algorithm ($8 \times$ SD of the spike-free baseline). To quantify SWR-related spiking, the number of spikes in n SWR epochs of 55 ms centered on the ripple maxima were determined. This dataset (N_1) was compared with spiking in n periods of identical duration (N_2) randomly sampled from the entire spike train, including periods with SWR epochs (Mann-Whitney U test; $\alpha = 0.001$). As a result, MCs were classified as responding or nonresponding during SWRs. The SWR maximum is the temporal reference in PETHs (bin width 5 ms; Figure 2F). The sum of spike counts S per time bin was divided by the sum m of SWRs observed and the bin width Δt ,

indicating spike rates ($SR = S/m/\Delta t$, i.e., the probability to observe a spike in a single trial for the chosen 5 ms time interval).

Individual synaptic inputs during cPSCs were detected by a derivative-peak time method (Figures 3C, S3B, and S3C): SWR-related cEPSCs and inverted cIPSCs were low-pass-filtered at 400 Hz and the derivative calculated. Of all derivative minima detected within a 60 ms window centered on the maximum of the ripple, the strongest 10% (i.e., 10% steepest slopes) were accepted as synaptic inputs. LFP signals were filtered at 127–300 Hz. Envelope and phase of the filtered signals were obtained by applying the Hilbert transform. The phase of excitatory or inhibitory inputs was determined as the respective Hilbert phase of the LFP at the time point of the steepest slopes. For each cell, an average phase vector described by its phase angle and strength was determined; the polar plots represent the resultant phase vectors of all analyzed cells.

Timing of cPSCs in double recordings was analyzed in a window of 15 ms surrounding the SWR maximum. Only significant SWR-related inputs were considered, and their delays at the time points of half-maximum amplitudes determined (see also Figures S3A and S4A).

The time-dependent power spectrum of the signal was computed using Morlet wavelet transform (Torrence and Compo, <http://atoc.colorado.edu/research/wavelets/>). Data are plotted as $\log(1 + \text{power})$. Frequency at maximum power is defined as the local maximum in the 127–300 Hz range.

Statistical analysis was performed in MATLAB or GraphPad Prism (GraphPad Software). Data are reported as mean \pm SEM or as medians. Box plots display the median and margin of error as the 10th and 90th percentiles. Comparisons were made using the two-tailed unpaired or paired *t* test, the Mann-Whitney U test, or ANOVA. The uniformity of phase angles was tested using Rayleigh's test with the CircStat toolbox (Berens, 2009). Fisher's Z transform was applied before comparing populations of correlation coefficients (Bortz and Schuster, 2010). Statistical significance is given as exact *p* values, with $\alpha \leq 0.05$ regarded as significant, unless stated otherwise.

SUPPLEMENTAL INFORMATION

Supplemental Information includes Supplemental Experimental Procedures and four figures and can be found with this article online at <https://doi.org/10.1016/j.celrep.2018.04.095>.

ACKNOWLEDGMENTS

We thank Susanne Rieckmann, Anke Schönherr, and Lisa Züchner for excellent technical assistance; Claire Cooper, Roberta Evangelista, Jörg G.R. Geiger, Friedrich W. Jochenning, Richard Kempter, Cheng-Chang Lien, Roger D. Traub, Imre Vida, and Christian Wozny for comments on the manuscript; and Richard Kempter, José R. Donoso, Janina Hesse, and Jan-Hendrik Schleimer for advice on data analysis. This study was supported by Deutsche Forschungsgemeinschaft (DFG) (SFB 958; Exc 257), Bundesministerium für Bildung und Forschung (BMBF) (Bernstein Center for Computational Neuroscience [BCCN] Berlin grant 01GQ1001A and Bernstein Focus Learning grant 01GQ0972; SMARTAGE).

AUTHOR CONTRIBUTIONS

Conceptualization, D.S. and N.M.; Formal Analysis, A.S., N.M., and I.W.; Investigation, A.S. and N.M.; Resources, D.S.; Data Curation, I.W., A.S., and N.M.; Writing – Original Draft, N.M.; Writing – Review & Editing, A.S., I.W., D.S., and N.M.; Visualization, N.M. and A.S.; Project Administration, N.M., D.S., and A.S.; Funding Acquisition, D.S. and N.M.

DECLARATION OF INTERESTS

The authors declare no competing interests.

Received: September 29, 2017

Revised: January 31, 2018

Accepted: April 23, 2018

Published: May 29, 2018

REFERENCES

- Acsády, L., Katona, I., Martínez-Guijarro, F.J., Buzsáki, G., and Freund, T.F. (2000). Unusual target selectivity of perisomatic inhibitory cells in the hilar region of the rat hippocampus. *J. Neurosci.* 20, 6907–6919.
- Aivar, P., Valero, M., Bellistri, E., and Menendez de la Prida, L. (2014). Extracellular calcium controls the expression of two different forms of ripple-like hippocampal oscillations. *J. Neurosci.* 34, 2989–3004.
- Amaral, D.G. (1978). A Golgi study of cell types in the hilar region of the hippocampus in the rat. *J. Comp. Neurol.* 182, 851–914.
- Berens, P. (2009). CircStat: a MATLAB toolbox for circular statistics. *J. Stat. Softw.* 37, 1–21.
- Berger, T.W., Semple-Rowland, S., and Basset, J.L. (1981). Hippocampal polymorph neurons are the cells of origin for ipsilateral association and commissural afferents to the dentate gyrus. *Brain Res.* 215, 329–336.
- Bortz, J., and Schuster, C. (2010). Statistik für Human- und Sozialwissenschaftler, Seventh Edition (Berlin-Heidelberg, Germany: Springer-Verlag).
- Both, M., Bähner, F., von Bohlen und Halbach, O., and Draguhn, A. (2008). Propagation of specific network patterns through the mouse hippocampus. *Hippocampus* 18, 899–908.
- Buckmaster, P.S., Strowbridge, B.W., and Schwartzkroin, P.A. (1993). A comparison of rat hippocampal mossy cells and CA3c pyramidal cells. *J. Neurophysiol.* 70, 1281–1299.
- Buckmaster, P.S., Wenzel, H.J., Kunkel, D.D., and Schwartzkroin, P.A. (1996). Axon arbors and synaptic connections of hippocampal mossy cells in the rat in vivo. *J. Comp. Neurol.* 366, 271–292.
- Buzsáki, G. (1986). Hippocampal sharp waves: their origin and significance. *Brain Res.* 398, 242–252.
- Buzsáki, G. (2015). Hippocampal sharp wave-ripple: a cognitive biomarker for episodic memory and planning. *Hippocampus* 25, 1073–1188.
- Buzsáki, G., and Eidelberg, E. (1981). Commissural projection to the dentate gyrus of the rat: evidence for feed-forward inhibition. *Brain Res.* 230, 346–350.
- Buzsáki, G., Buhl, D.L., Harris, K.D., Csicsvari, J., Czeh, B., and Morozov, A. (2003). Hippocampal network patterns of activity in the mouse. *Neuroscience* 116, 201–211.
- Danielson, N.B., Turi, G.F., Ladow, M., Chavlis, S., Petrantonakis, P.C., Poirazi, P., and Losonczy, A. (2017). In vivo imaging of dentate gyrus mossy cells in behaving mice. *Neuron* 93, 552–559.e4.
- Frotscher, M., Seress, L., Schwerdtfeger, W.K., and Buhl, E. (1991). The mossy cells of the fascia dentata: a comparative study of their fine structure and synaptic connections in rodents and primates. *J. Comp. Neurol.* 312, 145–163.
- Girardeau, G., Benchenane, K., Wiener, S.I., Buzsáki, G., and Zugaro, M.B. (2009). Selective suppression of hippocampal ripples impairs spatial memory. *Nat. Neurosci.* 12, 1222–1223.
- GoodSmith, D., Chen, X., Wang, C., Kim, S.H., Song, H., Burgalossi, A., Christian, K.M., and Knierim, J.J. (2017). Spatial representations of granule cells and mossy cells of the dentate gyrus. *Neuron* 93, 1–14.
- Hajos, N., Ellender, T.J., Zemankovics, R., Mann, E.O., Exley, R., Cragg, S.J., Freund, T.F., and Paulsen, O. (2009). Maintaining network activity in submerged hippocampal slices: importance of oxygen supply. *Eur. J. Neurosci.* 29, 319–327.
- Hajos, N., Karlócai, M.R., Németh, B., Ulbert, I., Monyer, H., Szabó, G., Erdélyi, F., Freund, T.F., and Gulyás, A.I. (2013). Input-output features of anatomically identified CA3 neurons during hippocampal sharp wave/ripple oscillation in vitro. *J. Neurosci.* 33, 11677–11691.
- Hashimoto, Y., Nasrallah, K., Jensen, K.R., Chávez, A.E., Carrera, D., and Castillo, P.E. (2017). LTP at hilar mossy cell-dentate granule cell synapses modulates dentate gyrus output by increasing excitation/inhibition balance. *Neuron* 95, 928–943.e3.
- Hedrick, T.P., Nobis, W.P., Foote, K.M., Ishii, T., Chetkovich, D.M., and Swanson, G.T. (2017). Excitatory synaptic input to hilar mossy cells under basal and hyperexcitable conditions. *eNeuro* 4 (6), ENEURO.0364-17.2017.

- Henze, D.A., and Buzsáki, G. (2007). Hilar mossy cells: functional identification and activity in vivo. *Prog. Brain Res.* 163, 199–216.
- Henze, D.A., Urban, N.N., and Barrionuevo, G. (2000). The multifarious hippocampal mossy fiber pathway: a review. *Neuroscience* 98, 407–427.
- Hosp, J.A., Strüber, M., Yanagawa, Y., Obata, K., Vida, I., Jonas, P., and Bartos, M. (2014). Morpho-physiological criteria divide dentate gyrus interneurons into classes. *Hippocampus* 24, 189–203.
- Hsu, T.T., Lee, C.T., Tai, M.H., and Lien, C.C. (2016). Differential recruitment of dentate gyrus interneuron types by commissural versus perforant pathways. *Cereb. Cortex* 26, 2715–2727.
- Hulse, B.K., Lubenov, E.V., and Siapas, A.G. (2017). Brain state dependence of hippocampal subthreshold activity in awake mice. *Cell Rep.* 18, 136–147.
- Jadhav, S.P., Kemere, C., German, P.W., and Frank, L.M. (2012). Awake hippocampal sharp-wave ripples support spatial memory. *Science* 336, 1454–1458.
- Jinde, S., Zsiros, V., Jiang, Z., Nakao, K., Pickel, J., Kohno, K., Belforte, J.E., and Nakazawa, K. (2012). Hilar mossy cell degeneration causes transient dentate granule cell hyperexcitability and impaired pattern separation. *Neuron* 76, 1189–1200.
- Karlócai, M.R., Kohus, Z., Káli, S., Ulbert, I., Szabó, G., Máté, Z., Freund, T.F., and Gulyás, A.I. (2014). Physiological sharp wave-ripples and interictal events in vitro: what's the difference? *Brain* 137, 463–485.
- Koniaris, E., Drimala, P., Sotiriou, E., and Papatheodoropoulos, C. (2011). Different effects of zolpidem and diazepam on hippocampal sharp wave-ripple activity in vitro. *Neuroscience* 175, 224–234.
- Kowalski, J., Geuting, M., Paul, S., Dieni, S., Laurens, J., Zhao, S., Drakew, A., Haas, C.A., Frotscher, M., and Vida, I. (2010). Proper layering is important for precisely timed activation of hippocampal mossy cells. *Cereb. Cortex* 20, 2043–2054.
- Kubota, D., Colgin, L.L., Casale, M., Brucher, F.A., and Lynch, G. (2003). Endogenous waves in hippocampal slices. *J Neurophysiol.* 89, 81–89.
- Larimer, P., and Strowbridge, B.W. (2008). Nonrandom local circuits in the dentate gyrus. *J. Neurosci.* 28, 12212–12223.
- Lasztóczy, B., Tukker, J.J., Somogyi, P., and Klausberger, T. (2011). Terminal field and firing selectivity of cholecystokinin-expressing interneurons in the hippocampal CA3 area. *J Neurosci.* 31, 18073–18093.
- Lee, A.K., and Wilson, M.A. (2002). Memory of sequential experience in the hippocampus during slow wave sleep. *Neuron* 36, 1183–1194.
- Li, X.G., Somogyi, P., Ylinen, A., and Buzsáki, G. (1994). The hippocampal CA3 network: an in vivo intracellular labeling study. *J. Comp. Neurol.* 339, 181–208.
- Lisman, J.E. (1999). Relating hippocampal circuitry to function: recall of memory sequences by reciprocal dentate-CA3 interactions. *Neuron* 22, 233–242.
- Lorente de Nó, R. (1934). Studies on the structure of the cerebral cortex. II. Continuation of the study of the ammonic system. *J. Psychol. Neurol.* 46, 113–177.
- Maier, N., Nimrich, V., and Draguhn, A. (2003). Cellular and network mechanisms underlying spontaneous sharp wave-ripple complexes in mouse hippocampal slices. *J. Physiol.* 550, 873–887.
- Maier, N., Morris, G., Johanning, F.W., and Schmitz, D. (2009). An approach for reliably investigating hippocampal sharp wave-ripples in vitro. *PLoS ONE* 4, e6925.
- Maier, N., Tejero-Cantero, A., Dorn, A.L., Winterer, J., Beed, P.S., Morris, G., Kempter, R., Poulet, J.F.A., Leibold, C., and Schmitz, D. (2011). Coherent phasic excitation during hippocampal ripples. *Neuron* 72, 137–152.
- Maier, N., and Kempter, R. (2017). Hippocampal Sharp Wave/Ripple Complexes—Physiology and Mechanisms. In *Cognitive Neuroscience of Memory Development*, N. Axmacher and B. Rasch, eds. (Switzerland: Springer International Publishing), pp. 227–249.
- Myers, C.E., and Scharfman, H.E. (2009). A role for hilar cells in pattern separation in the dentate gyrus: a computational approach. *Hippocampus* 19, 321–337.
- Neunuebel, J.P., and Knierim, J.J. (2012). Spatial firing correlates of physiologically distinct cell types of the rat dentate gyrus. *J. Neurosci.* 32, 3848–3858.
- Pangalos, M., Donoso, J.R., Winterer, J., Zivkovic, A.R., Kempter, R., Maier, N., and Schmitz, D. (2013). Recruitment of oriens-lacunosum-moleculare interneurons during hippocampal ripples. *Proc. Natl. Acad. Sci. U S A* 110, 4398–4403.
- Papatheodoropoulos, C., and Kostopoulos, G. (2002). Spontaneous GABA(A)-dependent synchronous periodic activity in adult rat ventral hippocampal slices. *Neurosci. Lett.* 319, 17–20.
- Patel, J., Schomburg, E.W., Berényi, A., Fujisawa, S., and Buzsáki, G. (2013). Local generation and propagation of ripples along the septotemporal axis of the hippocampus. *J. Neurosci.* 33, 17029–17041.
- Ribak, C.E., Seress, L., and Amaral, D.G. (1985). The development, ultrastructure and synaptic connections of the mossy cells of the dentate gyrus. *J. Neurocytol.* 14, 835–857.
- Scharfman, H.E. (1994a). Synchronization of area CA3 hippocampal pyramidal cells and non-granule cells of the dentate gyrus in bicuculline-treated rat hippocampal slices. *Neuroscience* 59, 245–257.
- Scharfman, H.E. (1994b). EPSPs of dentate gyrus granule cells during epileptiform bursts of dentate hilar “mossy” cells and area CA3 pyramidal cells in disinhibited rat hippocampal slices. *J. Neurosci.* 14, 6041–6057.
- Scharfman, H.E. (1994c). Evidence from simultaneous intracellular recordings in rat hippocampal slices that area CA3 pyramidal cells innervate dentate hilar mossy cells. *J. Neurophysiol.* 72, 2167–2180.
- Scharfman, H.E. (1995). Electrophysiological evidence that dentate hilar mossy cells are excitatory and innervate both granule cells and interneurons. *J. Neurosci.* 15, 179–194.
- Scharfman, H.E. (1996). Conditions required for polysynaptic excitation of dentate granule cells by area CA3 pyramidal cells in rat hippocampal slices. *Neuroscience* 72, 655–668.
- Scharfman, H.E. (2016). The enigmatic mossy cell of the dentate gyrus. *Nat. Rev. Neurosci.* 17, 562–575.
- Scharfman, H.E., and Myers, C.E. (2013). Hilar mossy cells of the dentate gyrus: a historical perspective. *Front. Neural Circuits* 6, 106.
- Scharfman, H.E., and Schwartzkroin, P.A. (1988). Electrophysiology of morphologically identified mossy cells of the dentate hilus recorded in guinea pig hippocampal slices. *J. Neurosci.* 8, 3812–3821.
- Scharfman, H.E., Kunkel, D.D., and Schwartzkroin, P.A. (1990). Synaptic connections of dentate granule cells and hilar neurons: results of paired intracellular recordings and intracellular horseradish peroxidase injections. *Neuroscience* 37, 693–707.
- Senzai, Y., and Buzsáki, G. (2017). Physiological properties and behavioral correlates of hippocampal granule cells and mossy cells. *Neuron* 93, 691–704.e5.
- Sík, A., Penttonen, M., and Buzsáki, G. (1997). Interneurons in the hippocampal dentate gyrus: an in vivo intracellular study. *Eur. J. Neurosci.* 9, 573–588.
- Soriano, E., and Frotscher, M. (1994). Mossy cells of the rat fascia dentata are glutamate-immunoreactive. *Hippocampus* 4, 65–69.
- Strowbridge, B.W., Buckmaster, P.S., and Schwartzkroin, P.A. (1992). Potentiation of spontaneous synaptic activity in rat mossy cells. *Neurosci. Lett.* 142, 205–210.
- Szabo, G.G., Du, X., Oijala, M., Varga, C., Parent, J.M., and Soltesz, I. (2017). Extended interneuronal network of the dentate gyrus. *Cell Rep.* 20, 1262–1268.
- Tukker, J.J., Lasztóczy, B., Katona, L., Roberts, J.D.B., Pissadaki, E.K., Dalezios, Y., Márton, L., Zhang, L., Klausberger, T., and Somogyi, P. (2013). Distinct dendritic arborization and in vivo firing patterns of parvalbumin-expressing basket cells in the hippocampal area CA3. *J. Neurosci.* 33, 6809–6825.
- Ylinen, A., Soltész, I., Bragin, A., Penttonen, M., Sík, A., and Buzsáki, G. (1995). Intracellular correlates of hippocampal theta rhythm in identified pyramidal cells, granule cells, and basket cells. *Hippocampus* 5, 78–90.